Int. J. Electrochem. Sci., 11 **(2016)** 6552 – 6563, doi: 10.20964/2016.08.58

International Journal of
ELECTROCHEMICAL
SCIENCE
www.electrochemsci.org

Short Communication

A Nano-Based Multilayer Separator for Lithium Rechargeable Battery

Jin Long, Xiwen Wang[*]*, Hongfeng Zhang, Jian Hu, Yi Wang*

State Key Lab of Pulp and Paper Engineering, South China University of Technology, Guangzhou Guangdong 510640, China
[*]E-mail: wangxw@scut.edu.cn

Received: 11 May 2016 / *Accepted:* 19 June 2016 / *Published:* 7 July 2016

The aim of the investigation is to improve the thermal stability of separator for lithium rechargeable battery, a three-layer separator mixture including PET nonwoven, cellulose nanofibers and ceramic coated layer was studied in this paper. The average diameter of the cellulose nanofibers was about 330nm, and the ceramic powder particles size was 0.1-3μm. The nanofiber was combined with the PET nonwoven substrate by wet-laid method. The ceramic particles were coated on the nanofiber layer by vacuum filtration. The max pore size of the separator was 750 nm, and the average pore size could reach 140nm. The porosity of the separator was 52%. At the same time, the separator has high affinity with electrolyte, in which electrolyte retention could reach 324%. The shrinkage of the separator was less than 1% under the treatment at 160℃ for 2 hours. The cell with the prepared multilayer separator exhibited excellent charge-discharge cycle performance.

Keywords: Lithium battery; Multilayer separator; Nano-based; Thermal stability

1. INTRODUCTION

Lithium rechargeable batteries are widely used as power sources in a lot of fields such as mobile phone, laptop computer and electric vehicles, etc. Positive electrode, negative, electrodes, electrolyte and separator are the critical components of lithium rechargeable batteries. The separator is a kind of porous electron insulating material which is placed between positive and negative electrodes to prevent physical contact of the electrodes while it can absorb electrolyte to allow free ionic transport. The separator is required to have thin thickness, small pore size, good wettability of electrolyte and good electrochemical stability. It can affect the battery performance including safety, energy density, charge and discharge performances [1-3].

At present, the commercial separator for lithium rechargeable battery are microporous polyolefin membranes, which are made of polypropylene(PP) or combinations of PP and polyethylene(PE) [4,5]. However, the fatal disadvantage of polyolefin membranes is their heat resistant property which is low melting temperature, 130℃ for PE and 160℃ for PP, respectively. When abnormal heat generation occurs, the polyolefin membranes may shrink, resulting in direct contact of electrodes. Hence, it is very important to increase the heat resistance of the separator and the safety of the battery. In recent years, some kinds of new materials such as electrospinning non-woven, wet-laid non-woven based on nanofibers and dry non-woven coated with ceramic powders have been developed for lithium rechargeable batteries to solve this shortcoming [6-23]. However, electrospinning non-woven had lower mechanical strength; it was very difficult to control the uniformity for dry non-woven coated with ceramic powder; most wet-laid non-woven separators based on nanofibers or nanofibers and ceramic powders were one or two-layer structure, it was very difficult to control the largest pore diameter for these wet-laid non-woven separator.

In this paper, the wet-laid method was employed to prepare the three-layers separator combining PET nonwoven, fibrillated cellulose nanofibers and ceramic powder particles, which had better heat resistant than PP separator. PET nonwoven acted as supporting material which offered adequate mechanical strength for the three-layers separator. Nanofibers were prepared by fibrillated Lyocell fiber, which could provide large porosity and control the main pore structure for the multilayer separator. Ceramic powder particles could reduce the average and largest pore size of the multilayer separator to prevent internal short circuit of the lithium rechargeable battery.

2. EXPERIMENTAL

2.1 Experimental material

(1) PET fiber 0.67dtex/6mm, Teijin, Japan.
(2) Lyocell fiber1.7dtex/4mm, Lenzing, Austria.
(3) Ceramic powder particles size 0.1-3μm, Deco Island Gold Technology Co. Ltd. China

2.2 Preparation of PET nonwoven

PET fibers were dispersed using deflaker (L&W 991509, Sweden) for 2000 revolutions(r), the nonwoven was obtained based on wet-laid method. Paper sheets were prepared with an ENJO-F-39.71 sheet machine made by Metrotec Spain. Then the PET nonwoven was pressed by double roller calendar (type-2230, KRK, Japan) under the linear pressure of 60kg/cm at 110°C. The targeted basis weight of membrane is 8g/m^2 and the thickness is 15μm.

2.3 Preparation of fibrillated Lyocell nanofibers

Lyocell fiber is obtained by spinning the dissolution of cellulose. Notably Lyocell fiber has the skin-core structure. Under the mechanical action, Lyocell fiber can be separated into nanofibers. These

kinds of nanofibers can be used in the preparation of micro-porous filter media to control the pore structure [24-28].

The fibers are beaten by PFI grinder for 30000r under the linear pressure of 1.00 N/mm with concentration of 10% following ISO5246/2. The prepared fibrillated pulp was dispersed in a pulp deflaker with concentration of 0.5% for 5000 revolutions. Then the fibrillated pulp suspension was classified by Bauer-McNett classifier (Figure 1) through five kinds of screens with 30, 50, 100, 120 and 200-mesh, respectively. The nanofibers passed through 200-mesh net was used to prepare multilayer separator.

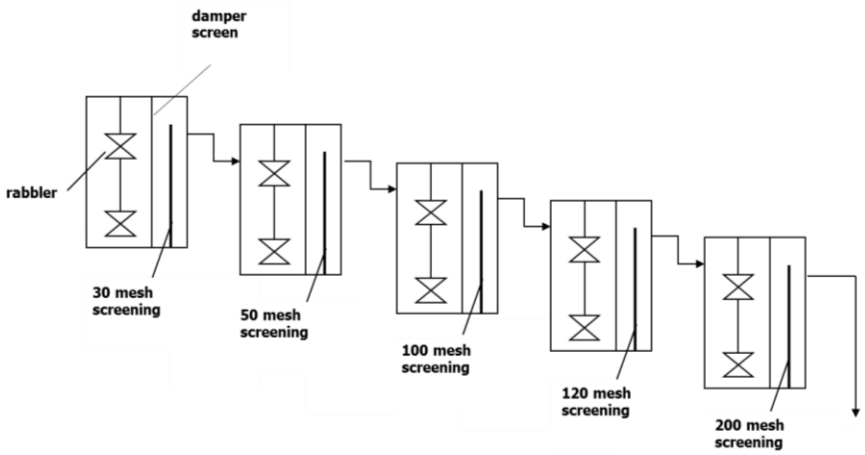

Figure 1. Schematic diagram of Bauer-McNett classifier

2.4 Multilayer separator preparation

Wet-laid (papermaking) processing was used to cover fibrillated nanofibers on the PET nonwoven, which acted as a substrate to supply the mechanical property for the separator. The nanofibers dosage was 7g per square meter with the concentration of 0.01%. The wet two-layer sheet was dried at the flat dryer at 105℃. After drying, the sheet was pressed by double roller calendar under the linear pressure of 20kg/cm at 25℃ in order to flat the sheet surface, then the Büchner funnel subjected to vacuum pump was employed to coat ceramic powder (10g per square meter with the concentration of 0.1%) on the cellulose nanofiber layer. Finally, the double roller calendar was used to decorate sheets surface again.

2.5 Characterization of nanofiber

2.5.1 Fiber length and distribution

The fiber length and distribution were tested using a fiber quality analyzer (Kajanni FS-300, Finland).

2.5.2 Specific surface area and fiber diameter

The specific surface area of the nanofiber was tested by B.E.T (SA3100, Beckman Coulter, USA) method according to Chinese standard GB/T19587.

Assumed that the microfiber was cylindrical and had the same length meanwhile, so the equivalent diameter of the fiber is calculated by Eq. (1):

$$D(nm)=4\times10^{6}/(\rho A-2/L) \quad (1)$$

Where ρ is fiber density (kg/m^3); A is fiber specific surface area (m^2/g); L represents fiber lengths (mm).

2.5.3 Crystallinity of nanofiber

X-ray diffraction (XRD) was employed to examine crystallinity of the nanofiber.

2.6 Characterization of Sparator

2.6.1 Basic weight and thickness

Basic weight and thickness were test according to the GB451-79 standard.

2.6.2 Pore size distribution and mean pore size

The separator pore size distribution and mean pore size were determined by Capillary Flow Porometer (CFP) manufactured by PMI (USA) and the wetting liquid was called Silwick.

2.6.3 Porosity

The porosity was determined by Eq. (2):

$$\text{Porosity}(\%)=(Wb-Wa)/(\rho e\times Vs)\times100\% \quad (2)$$

Where Wa and Wb are the weights of separator before and after soaked in the electrolyte, ρe is the density of electrolyte and Vs is the volume of separator.

2.6.4 Electrolyte wettability and retention

The wettability of electrolyte was examined by observing the wetting area of the separator surface when a drop of the electrolyte was dropped onto separator after 10 seconds.

The electrolyte retention was tested by Eq. (3) with the weights of separators before and after soaked in electrolyte for 10min.

$$\text{Electrolyte retention}(\%)=(Wb-Wa)/Wa\times100\% \quad (3)$$

Where Wa and Wb are the weights of separator before and after soaked in the electrolyte.

2.6.5 Thermal stability performances

The thermal shrinkage of multi-layer separator was evaluated by calculate the dimensional change after exposure to 160℃ for 2h.

The melting point of multi-layer separator was examined by Differential scanning calorimetry (DSC).

2.6.6 Scanning electron microscope (SEM) Observation

Scanning electron microscope was used to study the nanofiber and separator structures. A zeiss EVO 18 (zeiss, Germany) instrument was used. The samples were coated with gold and observed using an accelerating voltage of 10.0 kV.

2.6.7 Charge-discharge cycle performance

Coin cells (2032 type coin cell) were assembled in an argon filled glove box and a series of electrochemical performance were tested by MITS Pro Arbin Instruments.

3. RESULTS AND DISCUSSION

3.1 Nanofiber properties

As all known, when the fibers were shorter, it could be better dispersed in the water and the separator had better uniformity. The length distribution of nanofiber is shown in Figure 2, in which length mainly ranged from 0 to 1 mm. In this case, its average length was 0.20mm (shown in Table 1). So, it was suitable for preparing the multilayer separator.

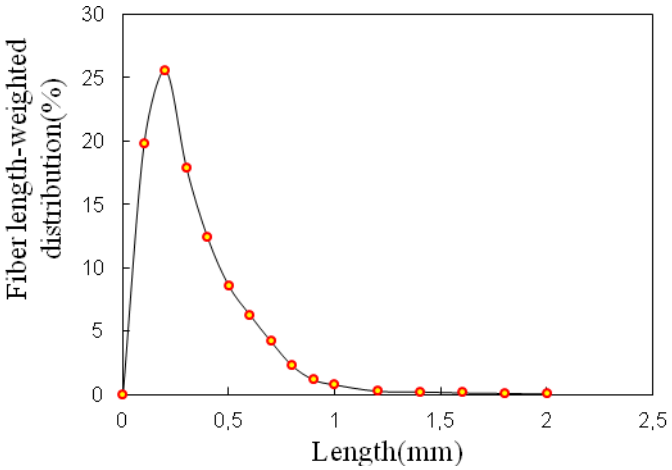

Figure 2. Length distribution of nanofibers

Table 1. The properties of prepared nanofiber.

	Specific surface area A (m^2/g)	Mean fiber diameter D (nm)	Average fiber length L(n) (mm)	Crystallinity (%)
Nanofiber	8.03	332	0.20	67

When the fibers were more fine, it could be easier to control the pore structure of the separator. The morphology of Lyocell fibrillated nanofiber is shown in Figure 3. It can be found that the fiber diameter was less than 1μm. However, it was hard to accurately measure the microfiber diameter due to its heterogeneity. Mean diameter (shown in Table 1) of the microfibers was calculated based on the equation (1) in which the specific surface area was tested by BET method. The average diameter can be as small as 332nm and the specific surface area was 8.03 m^2/g. So, the average pore diameter of the multilayer separator prepared by these nanofibers could reach to nanometer level, which could meet the basic requirements of the lithium rechargeable batteries separator.

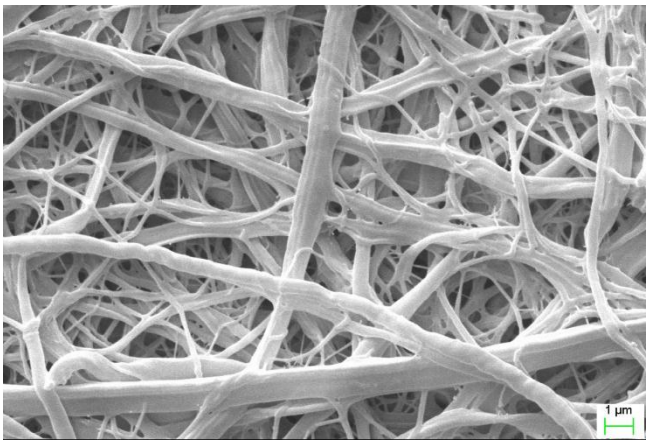

Figure 3. SEM image of Lyocell fibrillated nanofiber

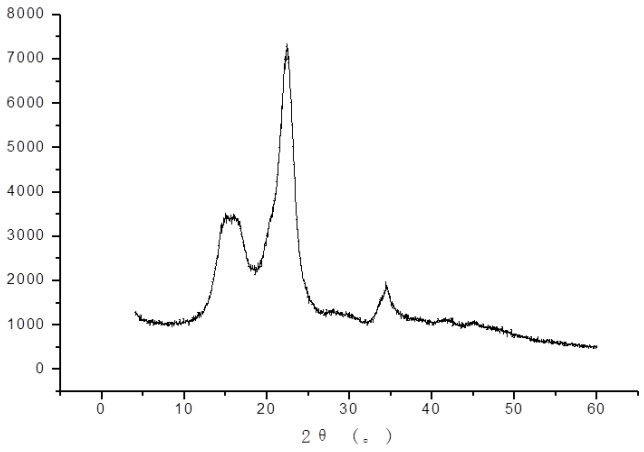

Figure 4. X-ray photograph of nanofiber

The crystallinity structure of cellulose nanofibers plays an important role in maintaining its dimensional stability even at high temperature or in the electrolyte. When the crystallinity of nanofibers was higher, the nanofibers would have better thermal stability. X-ray photograph of nanofiber is shown in Figure 4. The crystallinity is 67% based on the calculation, which suggested that the prepared nanofibers have good heat resistance.

3.2 Multilayer separator properties

Table2. summarized the properties of PET nonwoven, two-layer sheet (PET nonwoven and nanofibers), multilayer and PP separators. From this table, we can see that the nanofibers can significantly reduce the pore size of PET nonwoven. The average pore size of the multi-layer separator coated with ceramic particles could reach 140 nm, smaller than that of the two-layer sheet.

Table 2. Properties of PET nonwoven, Two-layer sheet, Multilayer and PP separators.

Separator samples	Thickness (μm)	Thermal shrinkage /160℃ for 2h (%)	Porosity (%)	Average pore size (μm)	Largest pore size (μm)	Electrolyte retention (%)
PET nonwoven	15.4	<1	57	52.45	105.68	362
Two-layer sheet	26.5	<1	54	0.27	1.45	385
Multi-layer separator	31.6	<1	52	0.14	0.75	324
PP Separator	30.4	25	42	0.05	0.20	185

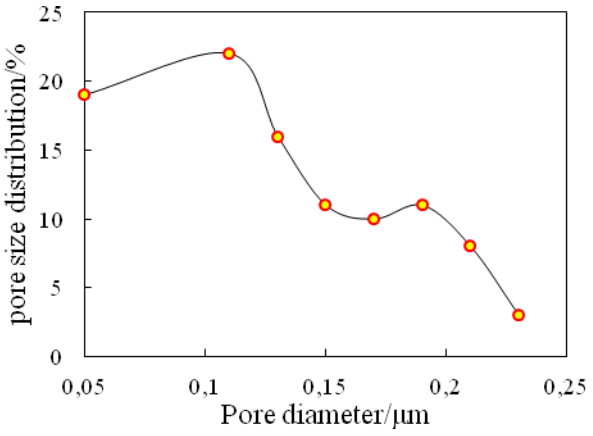

Figure 5. The pore size distribution of multilayer separator

The pore size distribution of multi-layer separator can be seen from Figure 5. It showed that the main pore size is less than 250 nm. The largest pore size of two-layer sheet was 1.45μm, bigger than

that (750 nm) of multi-layer separator. Hence, multi-layer separator had better uniformity than the two-layer sheet. Pankaj et al. discussed that the separator pore size less than 1μm could meet the needs of the lithium rechargeable battery to prevent internal short circuit [1,12]. Above all, the multi-layer separator is more suitable and safety for lithium rechargeable battery. The porosity and electrolyte retention of the multi-layer separator reached 52% and 324% respectively, which were bigger than that of PP separator with 42% porosity and 185% electrolyte retention.

Figure 6 shows cross section and surface SEM images of multilayer separator. We can find that the separator had an obvious three-layer structure. The ceramic particles were coated on the nanofiber layer, which could control the pore structure of the multilayer separator effectively. The thickness of ceramic particle, nanofiber and PET nonwoven layer was about 7μm, 11μm and 13μm, respectively. Meanwhile, three-dimensional network was constructed by compactly piled ceramic particles, where nanometer pores were supplied and well distributed over a wide area of the multi-layer separator. These nano-size pores could be filled with electrolyte and offer an effective ion transportation channels.

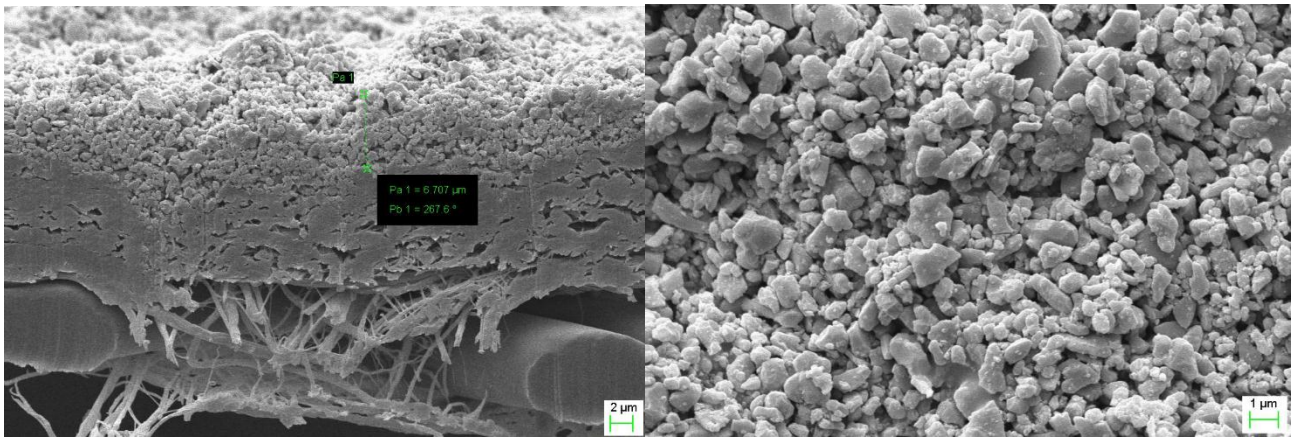

Figure 6. SEM images of multi-layer separator

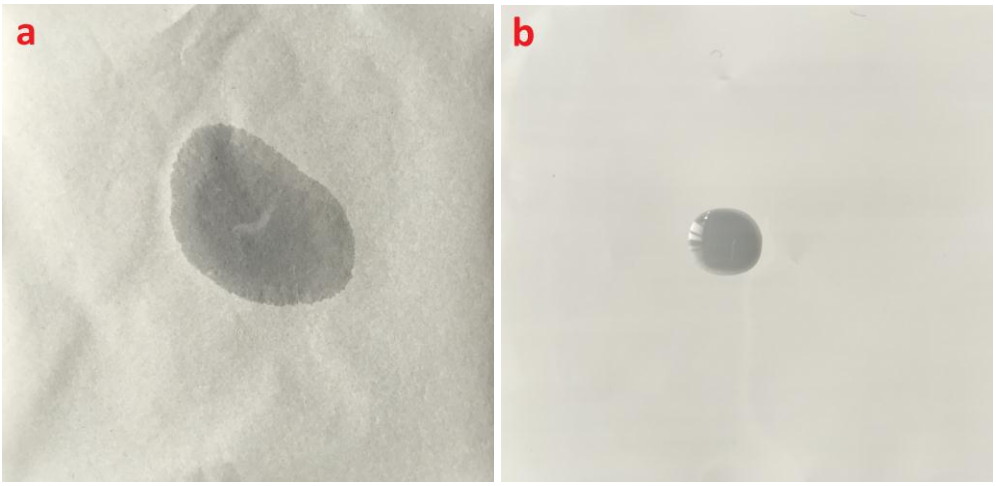

Figure 7. Comparison of electrolyte wettability of multi-layer separator (a) and PP separator (b)

It is clearly observed from Figure 7(a) that the electrolyte was absorbed by the multi-layer separator immediately. Moreover, the electrolyte easily spread over a wide area of the separator. However, it was difficult for PP separator to absorb electrolyte (shown in Figure 7(b)). This excellent electrolyte wettability of multi-layer separators can be attributed to its high (52%) porosity and unique nano-porous network channels, which contribute to capillary intrusion leading electrolyte into pores of multi-layer separators quickly [29-31].

As shown in Figure 8, the thermal shrinkage of multi-layer separator (Figure 8. (a)) and PP separator (Figure 8. (b)) were compared based on area dimensional change at the condition of 160℃ for 2h. Multilayer separator exhibited better thermal stability than PP separator, the shrinkage of multilayer separator was about 0% and that of PP separator was about 25%.

In order to further confirm thermal property of multilayer separator, DSC was used to examine melting point of multilayer separator as shown in Figure 9. Multilayer separator showed the endothermic peaks around 257℃, which was the melting point of PET. It indicated that multilayer separator had better thermal stability than PP and PE separator, which melting point were 163℃ and 130℃ [1], respectively. When the operating temperature of battery is over 160℃, thermal shrinkage (shown in figure 8.) of PP separator will lead to internal short circuit, especially for power lithium-ion battery, which is a serious threat to the battery safety. On the contrary, multilayer separator will never melt even at 250℃. Therefore, multilayer separator would be a fabulous material for battery to ensure the safety.

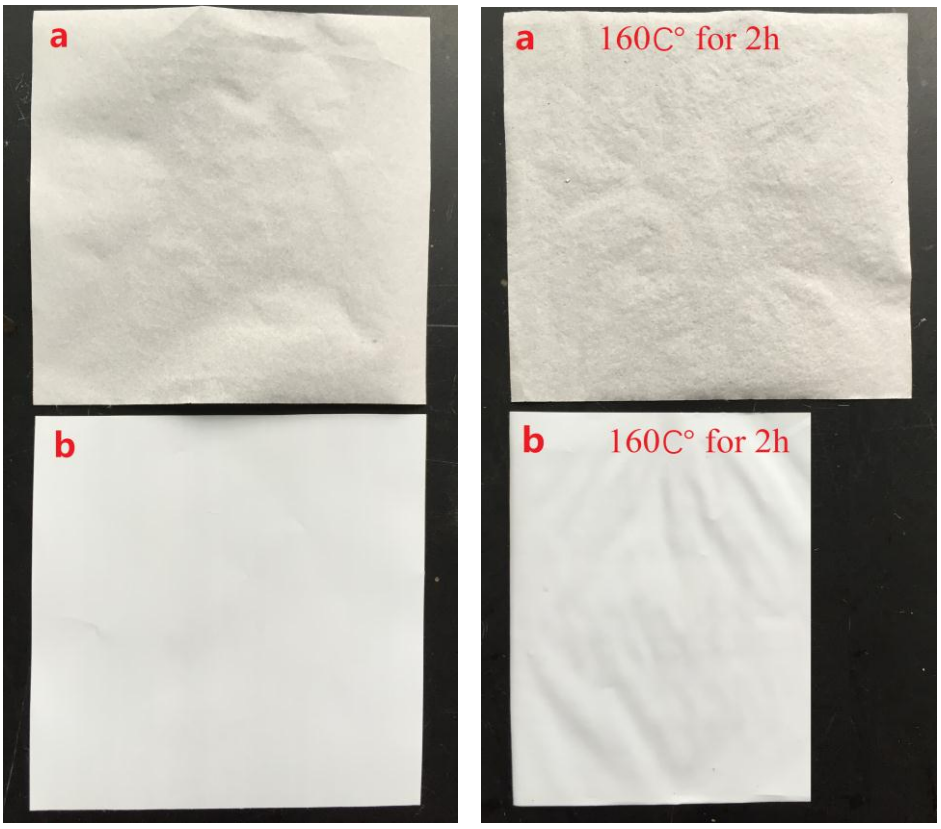

Figure 8. Thermal shrinkage of the multi-layer separator (a) and PP separator (b)

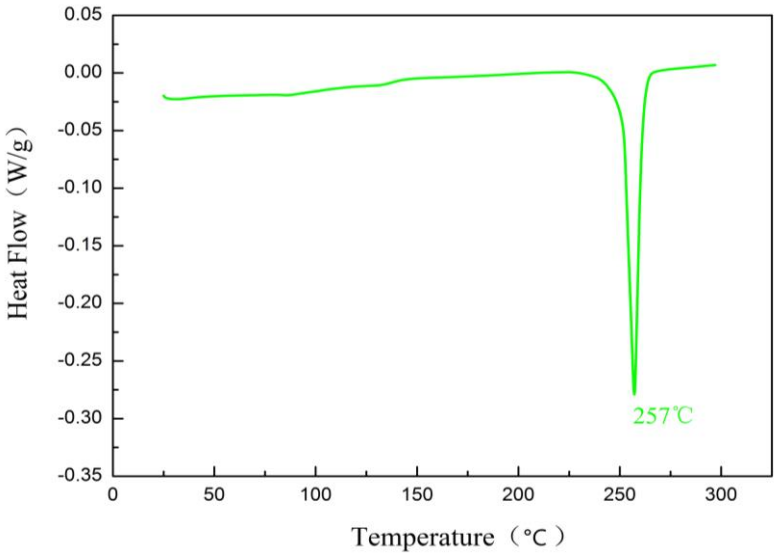

Figure 9. DSC diagram of multilayer separator

The cycle performance of cells with multilayer separator and PP separator is presented in Figure 10. The cells were cycle charged and discharged for 108 times, which were 6 times at 0.1C current density, 51 times at 1C current density and 51 times at 2C current density. The first charge and discharge specific capacity of the cell with multilayer separator reached 189.9 mAh.g-1 and 166.0 mAh.g-1, respectively. The discharge specific capacity at 0.1C current density was 159.1 mAh.g-1even after 6 times cycle, which was 95.8% of the initial discharge specific capacity. Moreover, the discharge specific capacity after 51 times cycle, was still 71.7% of the initial discharge specific capacity. The first charge specific capacity of the cell with PP separator was 179.8 mAh.g-1, the discharge specific capacity was 159.2 mAh.g-1; at 0.1C current density, after 6 times cycle, the discharge specific capacity was 149.7 mAh.g-1, which was 94.0% of the initial discharge specific capacity; at 1C current density, after 51 times cycle, the discharge specific capacity was 104.3 mAh.g-1, which was 65.5% of the initial discharge specific capacity.

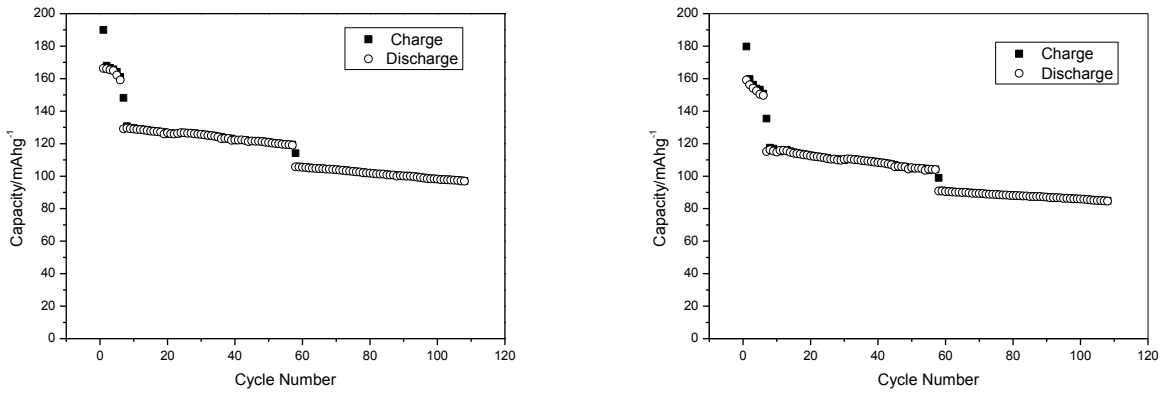

a b

Figure 10. The cycle performance of cells with multilayer separator(a) and PP separator(b)

In conclusion, the cell with multilayer separator exhibited better discharge specific capacity than that with PP separator after 108 times cycle. The reason was that multilayer separator had three-dimensional nanostructure which was constructed by nanofibers, ceramic particles and good electrolyte wettability, offering more flexible channels for Li-ion.

4. CONCLUSIONS

In this study, multilayer separators feathered with high porosity, excellent electrolyte wettability and high thermal tolerance were developed by wet-laid method. The separator had three layers including PET nonwoven, cellulose nanofibers and ceramic coated layer. The nanofibers were prepared by fibrillated Lyocell fibers. The nanofibers and ceramic particles could effectively control the pore size of the multilayer separator. The porosity of the separator could reach 52%. Meanwhile, the separator had high affinity with electrolyte, where electrolyte retention could reach 324%. Moreover, multilayer separator had better thermal stability than PP separator. The cell with multilayer separator exhibited better discharge specific capacity than that with PP separator after 108 times cycle. Hence, multilayer separator would be a fabulous promising alternative material for lithium rechargeable battery in the future.

ACKNOWLEDGEMENTS
The authors would like to thank the National Natural Science Foundation of China (31470608).

References

1. P. Arora and Z. Zhang, *Chem. Rev.*, 104 (2004) 4419-62.
2. D. Linden, T. B. Reddy, *Handbook of batteries*, 3rded, McMraw-Hill, New York (2002).
3. G. Venugopal, J. Moore, J. Howard and S. Pendalwar, *J. Power Sources*, 77 (1999) 34-41.
4. S. S. Zhang, J. Power Sources, 164 (2007) 351-364.
5. P. Kritzer, *J. Power sources*, 142 (2006) 1-6.
6. V. Hennige, H. Christian, H. Gerhard, *US patent*, US20050221165 (2005).
7. V. Hennige, H. Christian, H. Gerhard, *US patent*, US20050255769 (2005).
8. S. Augustin, V. Hennige, G. Hörpel and C. Hying, *Desalination*, 146(2002)23-28.
9. P. Kritzer, *J. Power sources*, 161 (2006) 1335-1340.
10. T. H. Cho, M. Tanaka, H. Onishi, Y. Kondo, T. Nakamura and H. Yamazaki, *J. Power sources*, 181 (2008) 155-160.
11. C. Yang, Z. Jia, Z. Guan and L. Wang, *J. Power sources*, 189 (2009) 716-720.
12. T. H. Cho, M. Tanaka, H. Ohnishi, Y. Kondo, M. Yoshikazu and T. Nakamura, *J. Power sources*, 195 (2010) 4272-4277.
13. H. Zhang, X. Wang and Y. Liang, *Heliyon*, 1.2 (2015) e00032.
14. J. Zhang, Q. Kong, Z. Liu, S. Pang, L. Yue, J. Yao, X. Wang and G. Cui, *Solid State Ionics*, s 245–246.5 (2013) 49-55.
15. J. H. Kim, J. H. Kim, E. S. Choi, H. K. Yu, J. H. Kim, Q. Wu, S. J. Chun, S.Y. Lee and S.Y. Lee, *J. Power sources*, 242.242 (2013) 533-540.
16. W. Xiao, Y. Gong, H. Wang, L. Zhao, J. Liu and C. Yan, *Ceramics International*, 41.10 (2015) 14223-14229.

17. J. H. Kim, J. H. Kim, E. S. Choi, J. H. Kim and S. Y. Lee, *Rsc Advances*, 4.97 (2014) 54312-54321.
18. X. Dong, W. Mi, L. Yu, Y. Jin and Y. S. Lin, *Microporous & Mesoporous Materials*, 226 (2016) 406-414.
19. W. Xiao, L. Zhao, Y. Gong, J. Liu, and C. Yan, *J. Memb. Sci*, 487 (2015) 221-228.
20. Q. Wang, *Electrochimica Acta*, 182 (2015) 334-341.
21. J. Shi, T. Shen, H. Hu, Y. Xia and Z. Liu, *J. Power sources*, 271 (2014) 134-142.
22. J. Shayapat, O. H. Chung and J. S. Park, *Electrochimica Acta*, 170 (2015) 110-121.
23. J. Lee, C. L. Lee, K. Park and I. D. Kim, *J. Power sources*, 248 (2014) 1211-1217.
24. W. S. Zhang, S. Okubayashi and T. Bechtold, *Carbohydrate Polymers*, 59 (2005) 173-179.
25. S. Q. Wang and Q. Z. Cheng, *J. Applied Polymer Science*, 113 (2009) 1270-1275.
26. S. S. Zeng, J. Hu, Y. Wang, L. Yun and T. Yu, *China Pulp & Paper*, 27 (2008) 16-19.
27. S. J. Chun, E. S. Choi, E. H. Lee, J. H. Kim and S. Y. Lee, *J. Mater. Chem.*, 22 (2012) 16618-16626.
28. I. V. Bletsos, J. R. Guckert and M. R. Levit, *US patent*, US8415262B2 (2013).
29. Hassoun, Jusef, P. Reale, and B. Scrosati, *J. Mater. Chem.*, 17 (2007) 3668-3677.
30. K. Xu, *Chem. Rev.*, 104 (2004) 4303-417.
31. E. S. Choi and S. Y. Lee, *J. Mater. Chem.*, 21 (2011) 14747-14754.